AD-A158 562 THE PARAMETERS OF ADIABATIC RAPID PASSAGE IN THE O-O HYPERFINE TRANSITION..(U) AEROSPACE CORP EL SEGUNDO CA CHEMISTRY AND PHYSICS LAB J C CAMPARO ET AL. 24 JUN 85 1/1

UNCLASSIFIED TR-0084A(5945-05)-4 SD-TR-85-20 F/G 20/8 NL

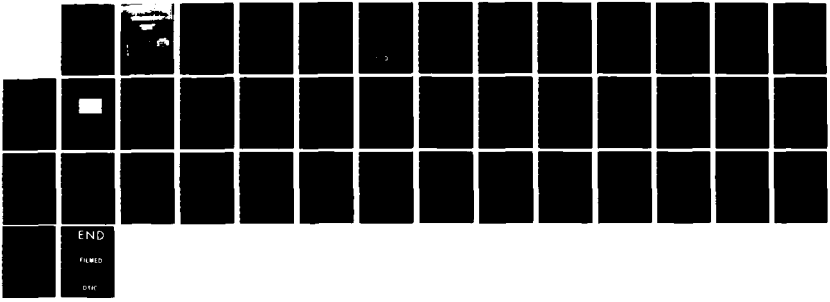

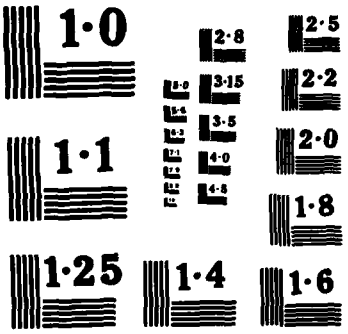

NATIONAL BUREAU OF STANDARDS
MICROCOPY RESOLUTION TEST CHART

AD-A158 562

Prepared for

SPACE DIVISION
AIR FORCE SYSTEMS COMMAND
Los Angeles Air Force Station
P.O. Box 92960, Worldway Postal Center
Los Angeles, CA 90009-2960

85 9 03 024

This report was submitted by The Aerospace Corporation, El Segundo, CA 90245, under Contract No. F04701-83-C-0084 with the Space Division, P.O. Box 92960, Worldway Postal Center, Los Angeles, CA 90009. It was reviewed and approved for The Aerospace Corporation by S. Feuerstein, Director, Chemistry and Physics Laboratory. Capt Matthew E. Hanson, YEZ, was the project officer for the Mission-Oriented Investigation and Experimentation (MOIE) Program.

This report has been reviewed by the Public Affairs Office (PAS) and is releasable to the National Technical Information Service (NTIS). At NTIS, it will be available to the general public, including foreign nationals.

This technical report has been reviewed and is approved for publication. Publication of this report does not constitute Air Force approval if the report's findings or conclusions. It is published only for the exchange and stimulation of ideas.

Matthew E. Hanson CAPT, USAF

MATTHEW E. HANSON, Capt, USAF
Ch, Satellite Development Branch
SD/YEZ

Joseph Hess

JOSEPH HESS, GM-15
Director, AFSTC West Coast Office
AFSTC/WCO OL-AB

UNCLASSIFIED

SECURITY CLASSIFICATION OF THIS PAGE (When Data Entered)

REPORT DOCUMENTATION PAGE

READ INSTRUCTIONS BEFORE COMPLETING FORM

1. REPORT NUMBER: SD-TR-85-20

2. GOVT ACCESSION NO.: A158 562

3. RECIPIENT'S CATALOG NUMBER:

4. TITLE (and Subtitle): THE PARAMETERS OF ADIABATIC RAPID PASSAGE IN THE 0-0 HYPERFINE TRANSITION OF ^{87}Rb

5. TYPE OF REPORT & PERIOD COVERED:

6. PERFORMING ORG. REPORT NUMBER: TR-0084A(5945-05)-4

7. AUTHOR(s): James C. Camparo and Robert P. Frueholz

8. CONTRACT OR GRANT NUMBER(s): F04701-83-C-0084

9. PERFORMING ORGANIZATION NAME AND ADDRESS: The Aerospace Corporation, El Segundo, CA 90245

10. PROGRAM ELEMENT, PROJECT, TASK AREA & WORK UNIT NUMBERS:

11. CONTROLLING OFFICE NAME AND ADDRESS: Space Division, Los Angeles Air Force Station, Los Angeles, CA 90009-2960

12. REPORT DATE: 24 June 1985

13. NUMBER OF PAGES: 40

14. MONITORING AGENCY NAME & ADDRESS (if different from Controlling Office):

15. SECURITY CLASS. (of this report): Unclassified

15a. DECLASSIFICATION/DOWNGRADING SCHEDULE:

16. DISTRIBUTION STATEMENT (of this Report): Approved for public release; distribution unlimited.

17. DISTRIBUTION STATEMENT (of the abstract entered in Block 20, if different from Report):

18. SUPPLEMENTARY NOTES:

19. KEY WORDS (Continue on reverse side if necessary and identify by block number): Adiabatic rapid passage; Atomic line shapes; Quantum mechanics.

Cont'd

20. ABSTRACT (Continue on reverse side if necessary and identify by block number)

The parameters of adiabatic rapid passage (ARP) in the ground-state 0-0 hyperfine transition of ^{87}Rb have been investigated. These parameters relate to how adiabatic and how rapid the passage through resonance must be in order to maximize the degree of population reversal. We find both experimentally and theoretically that the adiabaticity requirement is rather weak, and that once satisfied, it is more important to pass through the resonance rapidly. Furthermore, interpreting our results in the Bloch

Cont'd

DD FORM (FACSIMILE) 1473

UNCLASSIFIED

SECURITY CLASSIFICATION OF THIS PAGE (When Data Entered)

19. KEY WORDS (Continued)

20. ABSTRACT (Continued)

vector model of ARP, we find that the Bloch vector is only required to precess a half revolution about the effective field in order to follow a 90° change in the direction of that field. The applicability of the present results to ARP in general is discussed. Originator supplied keywords included

CONTENTS

I. INTRODUCTION 3

II. EXPERIMENTAL PROCEDURE 7

A. General Description 7

B. Details of the Experimental Arrangement 7

C. Measurement of the Rabi Frequency, the Dephasing Rate, and the Ratio (T_1/T_2) 12

III. RESULTS 17

IV. THEORY 19

A. The ^{87}Rb Density-Matrix Solution 19

B. The Two-Level Density Matrix 21

C. Analytic Approximation 21

V. DISCUSSION 27

A. Comparison of the Experimental Result and the Full ^{87}Rb Density-Matrix Calculations 27

B. Comparison of the ^{87}Rb Density-Matrix Calculations and the Spin-1/2 Numerical Solutions 27

C. Qualitative Analysis of the Results 28

VI. SUMMARY 31

REFERENCES 33

APPENDIX: THE RELAXATION OF THE TRANSMISSION LINE SHAPE LINEWIDTH TO THE PEAK AXIAL MICROWAVE RABI FREQUENCY 35

DTIC
ELECTE
SEP 5 1985
S D
B

Accession For
NTIS GRA&I ☑
DTIC TAB ☐
Unannounced ☐
Justification
By
Distribution/
Availability Codes
Dist | Avail and/or Special
A-1

DTIC COPY INSPECTED

FIGURES

1. Schematic Energy-Level Diagram of ^{87}Rb, Showing the Radiative Transitions of Interest 8

2. Experimental Arrangement for the ARP Experiments 9

3. The Absorption Signal versus Microwave Frequency, as Measured by the Transmitted Light Intensity 11

4. Plot of the Measured Half-Width Half-Maximum (HWHM) versus the square Root of the Normalized Microwave Power Fed into the Cavity 14

5. Plots of the Adiabaticity Parameter η_0 and the Rapidity parameter ξ_0 as Functions of the Normalized Rabi Frequency $\omega_1 T_2$ 18

6. An Example of the Discrete Set of Data Points Generated by our Model 22

7. In the Rotating Coordinate System the Spin Vector Precesses about an Effective Field H_{eff}, as Shown in (a); the Precessional Frequency is $\hat{\Omega}$, as Shown in (b); and (c) Depicts the Precessional Angle Swept Out during the Passage through Resonance, $\Delta\phi$, as the Effective Field is Swept from $-z$ to $+z$ 25

TABLE

1. Relevant Experimental Data 17

I. INTRODUCTION

It is well known that when an electromagnetic field, coupling two levels of an atomic or molecular system, has its frequency swept across resonance, population reversal can occur as a result of the coherent transient phenomenon known as adiabatic rapid passage (ARP).[1] For this phenomenon to occur, the frequency sweep rate is required to be "rapid" with respect to the relaxation processes occuring in the system, and at the same time slow enough so that the system can follow the frequency sweep "adiabatically." Though ARP was first observed in nuclear magnetic resonance (NMR),[2] the phenomenon is quite general and has been demonstrated in electron paramagnetic resonance (EPR) experiments[3] and in both one-[4,5] and two-[6] photon optical studies. The present investigations treat ARP in the ^{87}Rb hyperfine transition, where optical pumping produces a population imbalance in the ground-state hyperfine levels, and where the influence of a microwave frequency swept across the hyperfine resonance is monitored by the transmitted intensity of the optical pumping laser. Though the hyperfine transition of ^{87}Rb is interesting in its own right, our prime concern was to obtain a better understanding of ARP processes in general.

The conditions on the frequency sweep rate for ARP are typically written as

$$\frac{\omega_1}{T_2} \ll \left|\frac{d}{dt}(\omega - \omega_0)\right| \ll \omega_1^{\,2} \tag{1}$$

where ω_1 is the Rabi frequency, T_2 the dephasing time, and $(\omega - \omega_0)$ the detuning between the resonant frequency and the frequency of the perturbing field. Defining β as the rate of change of the resonance condition, Eq. (1) can be written in the dimensionless form

$$\frac{\omega_1}{\beta\, T_2} \ll 1 \ll \frac{\omega_1^2}{\beta} \tag{2}$$

Cont'd DD1473

where the terms on the left- and right-hand sides of Eq. (2) specify the sweep requirements of rapidity and adiabaticity, respectively. Whereas population reversal is typically stated as the result of ARP when these two conditions are satisfied, in all real systems, with finite values of T_2, total population reversal can only occur when the conditions are maximally satisfied, i.e., when the Rabi frequency is infinite. In the laboratory this can never be accomplished; instead, "we take T_2 as nature gives it"[2] and work with some finite value of ω_1. This, however, raises a question: How should the sweep rate β be chosen in order to maximize the population reversal? Analysis of this question in the ^{87}Rb system and application of the results to the generic ARP process is the thrust of this paper.

To aid in the analysis of ARP two parameters are defined. ξ_0, the rapidity parameter, and η_0, the adiabaticity parameter, are equal to the terms on the left- and right-hand sides of Eq. (2), respectively, which maximize population reversal during ARP. To facilitate general applicability of the current results, these two parameters are analyzed in terms of a dimensionless quantity, the normalized Rabi frequency $\omega_1 T_2$, and from Eq. (2) we see that

$$\eta_0/\xi_0 = \omega_1 T_2 \tag{3}$$

Essentially, we want to determine the behavior of ξ_0 and η_0 as functions of the normalized Rabi frequency, and to understand on a conceptual level the physics behind this behavior. Though Eq. (2) states the general conditions for ARP, it gives no clue as to the behavior we seek; furthermore, we have found no detailed discussion of this behavior in the literature.

It is particularly interesting to study ARP in the ground-state hyperfine levels of ^{87}Rb, as this is not a two-level system. The two hyperfine levels of ^{87}Rb, F = 1 and F = 2, are composed of Zeeman sublevels, of which only the $m_F = 0$ levels are coupled by the sweeping radiation field. In addition to experimental study, theoretical analyses are conducted at several levels. First, a detailed density-matrix analysis of the entire ^{87}Rb hyperfine system is performed. The system is then reanalyzed in terms of a strict two-level

model. This analysis provides insight into how applicable the current experimental results are to other two-level ARP processes. Finally, a simplified analysis of the two-level system yields an approximate closed-form result for the degree of population reversal during ARP. From this result we feel physical insight into the ARP process is gained.

II. EXPERIMENTAL PROCEDURE

A. GENERAL DESCRIPTION

In the present experiment we investigated the conditions for ARP in the ground state 0-0 hyperfine transition of ^{87}Rb; Fig. 1 shows the radiative interactions of interest. A single-mode diode laser (Mitsubishi ML-4101), tuned to one of the D_1 hyperfine resonance lines at 794.7 nm, was used to optically pump atoms from the $5^2S_{1/2}$ (F = 2) Zeeman manifold into the $5^2S_{1/2}$ (F = 1) Zeeman manifold. The Doppler-broadened absorption linewidth (~500 MHz) was greater than both the laser linewidth (~100 MHz) and the Zeeman splitting (<700 kHz). Thus optical pumping occurred from only the F = 2 hyperfine state, but from all Zeeman sublevels of that state.[9]

The transmitted intensity of the laser through the Rb vapor was used to determine the density of atoms in the F = 2 level, and in steady-state, in the absence of the microwave field, this intensity is a maximum. By sweeping a microwave field across the 0-0 hyperfine transition, atoms in the (F = 1, m_F = 0) state were transferred into the (2,0) state, and the resulting change in the transmitted laser intensity was a measure of the number of atoms transferred. For a fixed microwave field strength, the sweep rate of the microwave frequency was adjusted so we could observe the largest change in the transmitted light intensity. Thus, we were able to measure the sweep rate that maximized the population reversal as a function of microwave field strength or, equivalently, the microwave Rabi frequency.

B. DETAILS OF THE EXPERIMENTAL ARRANGEMENT

The experimental apparatus is shown schematically in Fig. 2. A Corning 7070 glass absorption cell that contained an excess of ^{87}Rb metal and N_2 at 10 Torr was situated in a TE_{011} cylindrical microwave cavity (R = 2.8 cm) tuned to the ^{87}Rb ground-state hyperfine transition frequency, 6834 MHz. The N_2 was present in order to quench the Rb fluorescence, and to act as a buffer to reduce the effect of collisions with the cell walls. A static magnetic field of a few hundred milligauss was applied parallel to the cavity axis in order

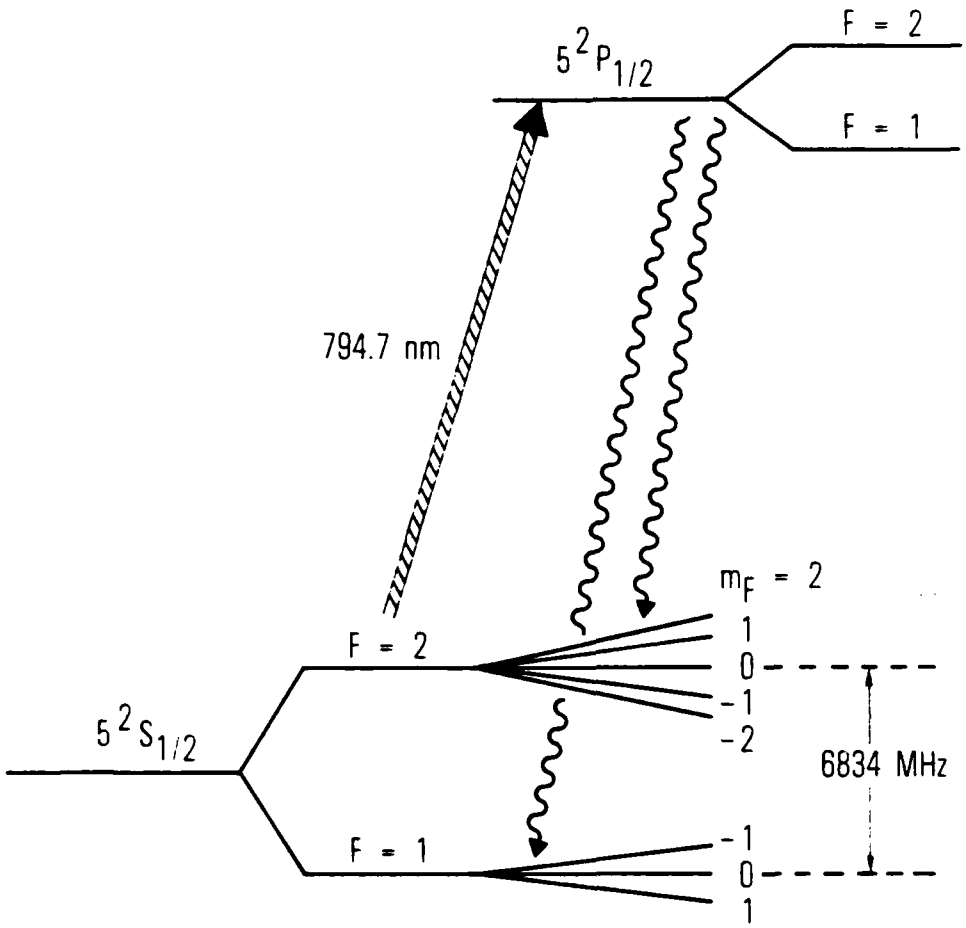

Fig. 1. Schematic Energy-Level Diagram of ^{87}Rb, Showing the Radiative Transitions of Interest.

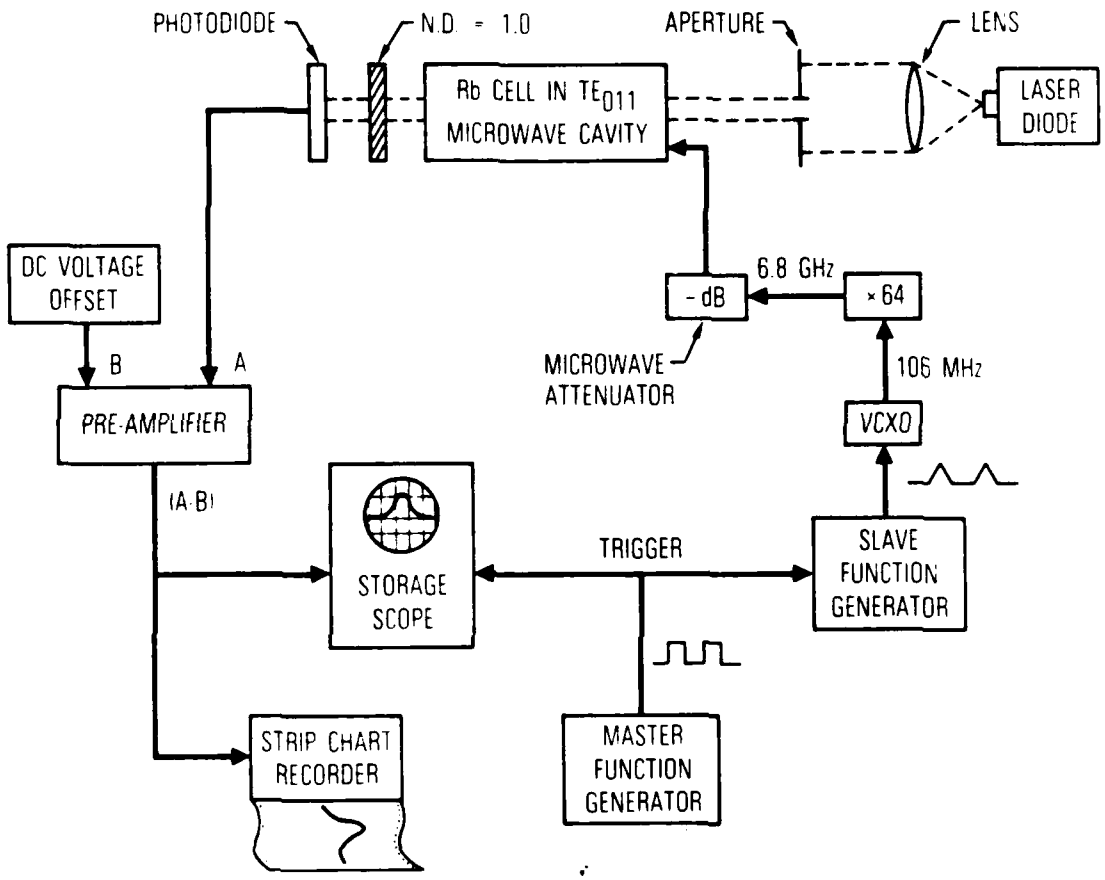

Fig. 2. Experimental Arrangement for the ARP Experiments. In order to measure the slow-passage linewidth in the limit of zero microwave power, the preamp was replaced by a lock-in amplifier, and the microwaves were chopped at a low frequency.

to define the quantization axis, and to split the Zeeman levels so that only the 0-0 transition was induced by the microwaves. The cavity and cell were thermostatically controlled to ±0.1°C at about 37°C, and were surrounded by three layers of magnetic shielding.

The diode laser emission was collimated by a short-focal-length lens to a diameter of ~0.8 cm, so that an aperture (~0.2 cm diameter) allowed only the central portion of the laser beam to enter the absorption cell. Since the radial profile of the laser emission is well approximated by a Gaussian, and since the vapor was optically thin ($[Rb]\sigma\ell = 0.56$),[10] the intensity distribution in the cell volume was expected to be fairly uniform. These precautions were necessary in order to make the effects of light-induced inhomogeneous broadening negligible.[11]

The microwave frequency sweep was generated by applying a voltage ramp to a calibrated voltage-controlled crystal oscillator (VCXO), whose output at ~106 MHz was multiplied to the ^{87}Rb hyperfine frequency region and then attenuated before being allowed to power the microwave cavity. The voltage ramp amplitude and duration determined the frequency sweep rate of the 6834-MHz microwaves, and these were adjusted to produce a maximum signal amplitude on the oscilloscope; a typical ARP signal is shown in Fig. 3. The sweep rate that produces the maximum ARP signal is designated β_0. In order to ensure that our measured β_0 corresponded to a single pass through resonance, starting with the system in a steady-state condition, the ramp voltage to the VCXO was supplied by a "slave" function generator whose output was triggered every 2 sec by a "master" function generator. Since our experimentally determined pumping and relaxation times were on the order of milliseconds, steady-state conditions were attained in the time between each passage.

As a result of the presence of the buffer gas, the atoms are considered as essentially "frozen" in place;[11] therefore, they experience a microwave Rabi frequency determined by their position in the TE_{011} mode:[12]

$$\omega_1(r,z) = \omega_{1p}\left|J_0\left(3.832\,\frac{r}{R}\right)\right|\sin\left(\frac{\pi z}{L}\right) \tag{4}$$

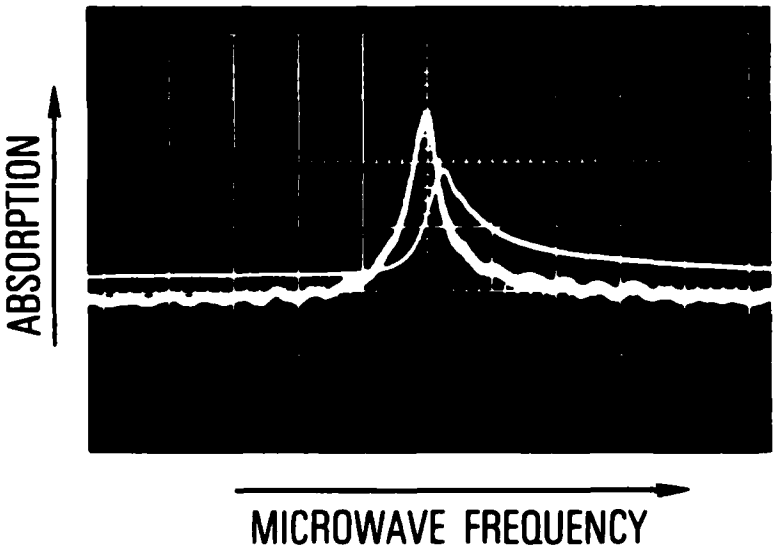

Fig. 3. The Absorption Signal versus Microwave Frequency, as Measured by the Transmitted Light Intensity. The symmetric line shape corresponds to a slow passage through resonance. The asymmetric line shape, five times larger than actually shown, corresponds to a rapid passage that maximized the population reversal for an average Rabi frequency in the cavity of ~2.3 kHz. Note that the maximum of the fast-passage signal occurs when the microwaves have swept approximately one half-width beyond resonance.

where R and L are, respectively, the cavity radius and length. The experiment is arranged so that the laser beam travels down the center of the cavity, and because the laser beam diameter is so much smaller than the cavity diameter, the radial variation of the Rabi frequency for those atoms probed by the laser is only ~0.5%. Therefore, the Rabi frequency may be accurately approximated by

$$\omega_1(r,z) \simeq \omega_1(0,z) = \omega_{1p} \sin\left(\frac{\pi z}{L}\right) \tag{5}$$

Since all the atoms in the laser beam contribute to the signal amplitude, we somewhat arbitrarily associate our measured optimum sweep rate with an average of the Rabi frequency over the length of the cavity:

$$\langle\omega_1\rangle = \frac{2}{\pi}\,\omega_{1p} \tag{6}$$

$\langle\omega_1\rangle$ is then the Rabi frequency used in determining the normalized Rabi frequency $\omega_1 T_2$ associated with the values of η_0 and ξ_0.

The absolute magnitude of the Rabi frequency within the cavity is not obtained from the rapid-passage experiment. Rather, the quantity over which experimental control is maintained is the microwave power entering the cavity. Through the use of variable microwave attenuators, precise microwave power levels are allowed into the cavity. To relate these power levels to absolute Rabi frequencies requires additional measurements.

C. MEASUREMENT OF THE RABI FREQUENCY, THE DEPHASING RATE, AND THE RATIO (T_1/T_2)

It is well known that the half width at half maximum (HWHM), $\Delta\omega_{1/2}$, of the transition line shape in a two-level system is given by

$$\Delta\omega_{1/2} = [(1/T_2)^2 + (T_1/T_2)\,\omega_1^2]^{1/2} \tag{7}$$

where T_1 and T_2 are, respectively, the longitudinal and transverse relaxation times. For the case of the 0-0 hyperfine transition in an alkali, the expression for $\Delta\omega_{1/2}$ can be put in the same form as Eq. (7). However, because of

the presence of the other Zeeman sublevels, T_1 is no longer the standard longitudinal relaxation time, but becomes a complicated function of the photon absorption rate B and a phenomenological relaxation rate γ.[13] The dephasing rate $1/T_2$ is, however, related to B and γ in a fairly simple way:

$$\frac{1}{T_2} = \frac{B}{2} + \gamma \tag{8}$$

For the transmission line shape in our experiment, the Rabi frequency appearing in Eq. (7) is well approximated by ω_{1p}; this is discussed in the Appendix. Line shapes were recorded on a strip chart for each attenuation level of the microwave power. Care was taken to ensure that these line shapes corresponded to a slow passage through resonance. Thus, once the dephasing rate and the ratio (T_1/T_2) were determined, we could extract ω_{1p} from our linewidth measurements.

As implied by Eq. (7), the dephasing rate is given by the transmission linewidth in the limit of zero Rabi frequency. To perform the measurement we replaced the preamp with a lock-in amplifier and chopped the microwaves with a diode switch placed after the microwave attenuator. In this way we could measure linewidths at very low microwave power levels and extrapolate these measurements to zero microwave power. The results of these measurements are shown in Fig. 4, and the solid line is a least-squares fit of the data to the form of Eq. (7). This procedure yielded an extrapolated dephasing rate of 52 Hz.

In order to determine T_1/T_2 it was necessary to know both B and γ individually. This was accomplished by using our known value of the dephasing rate, and a measurement of the fractional population ζ in the F = 2 ground-state hyperfine level as a result of optical pumping. The transmitted intensity of the laser beam was measured for the laser tuned off and on resonance:

$$\ln[I(\text{off})/I(\text{on})] = \zeta\ [\text{Rb}]\ \sigma\ell \tag{9}$$

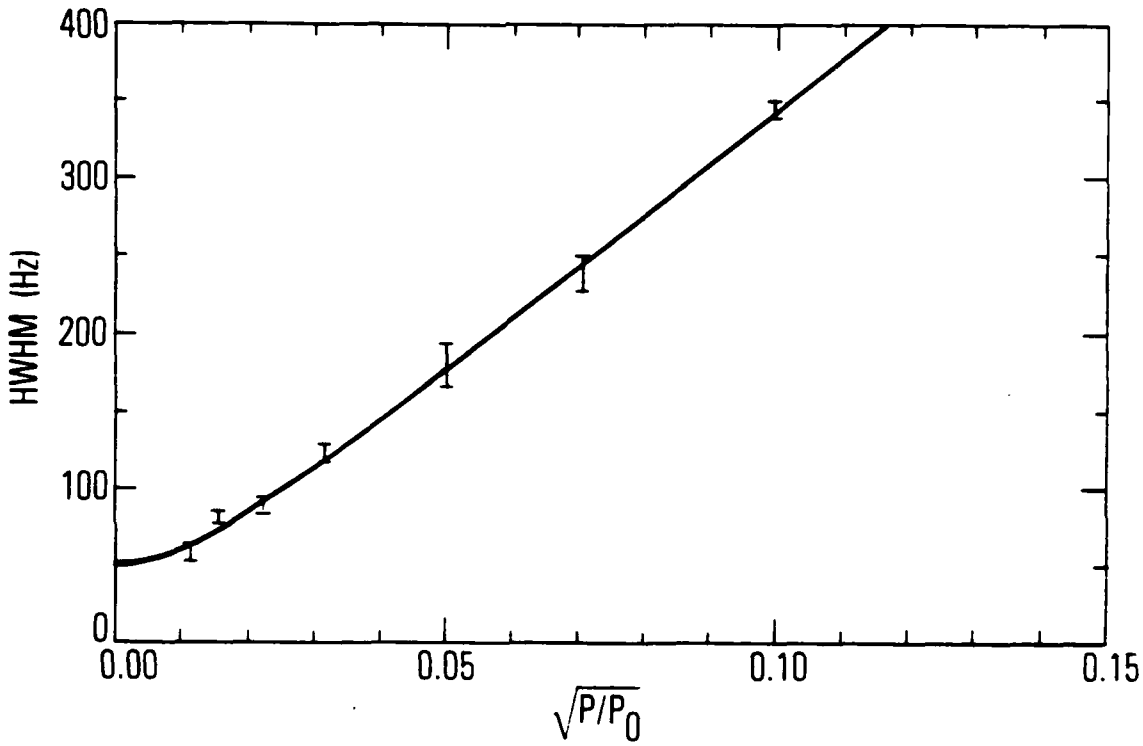

Fig. 4. Plot of the Measured Half-Width Half-Maximum (HWHM) versus the Square Root of the Normalized Microwave Power Fed into the Cavity. The solid line is a least-squares fit of the data, yielding an intercept of 52 Hz.

and yielded the result $\zeta = 0.31$.[14] The homogeneous density-matrix rate equations for ^{87}Rb were then solved in steady state,[11] and the pumping rate and relaxation rate were varied so as to give calculated results consistent with our experimental determination of $1/T_2$ and ζ. In this way we obtained values of 60 Hz and 22 Hz for B and γ, respectively, which resulted in $T_1/T_2 = 1.34$.

III. RESULTS

Using the various values of ω_{1p} and β_0, it is a straightforward procedure to evaluate the corresponding rapidity and adiabaticity parameters. The relevant experimental data, and the resulting determination of ξ_0 and η_0, are collected in Table 1. Figure 5 shows these values plotted as functions of normalized Rabi frequency, $\omega_1 T_2$. Essentially, this figure shows, as a function of Rabi frequency, how rapid and how adiabatic the passage through resonance must be in order to maximize the degree of population reversal.

The most striking feature of the figure is the disparity in the rate of change of the parameters as a function of Rabi frequency. The adiabaticity parameter, while greater than unity (implying satisfaction of the adiabatic condition), increases very slowly. However, the rapidity parameter decreases at a very much faster rate. This is not at all obvious from the conditions for ARP, and in fact we had naively expected the rapidity and adiabaticity parameters to change at approximately the same rate. The implication of these results is that while it is important to satisfy the adiabatic condition in ARP, once it is satisfied it is more important to pass through the resonance as rapidly as possible.

Table 1. Relevant Experimental Data

Microwave Attenuation Level, db	β_0, rad/s^2	$\Delta\omega_{1/2}$, rad/s	ω_{1p}, rad/s	$\langle\omega_1 T_2\rangle$	ξ_0	η_0
3	1.1×10^8	2.7×10^4	2.3×10^4	45	0.043	1.9
6	6.7×10^7	1.9×10^4	1.7×10^4	33	0.053	1.7
10	2.5×10^7	1.2×10^4	1.0×10^4	19	0.083	1.6
13	1.3×10^7	8.5×10^3	7.4×10^3	14	0.12	1.7
16	6.7×10^6	6.0×10^3	5.2×10^3	10	0.16	1.6
20	3.0×10^6	3.8×10^3	3.3×10^3	6.4	0.23	1.5
23	1.0×10^6	2.7×10^3	2.3×10^3	4.5	0.48	2.1
26	5.7×10^5	1.9×10^3	1.6×10^3	3.1	0.58	1.8

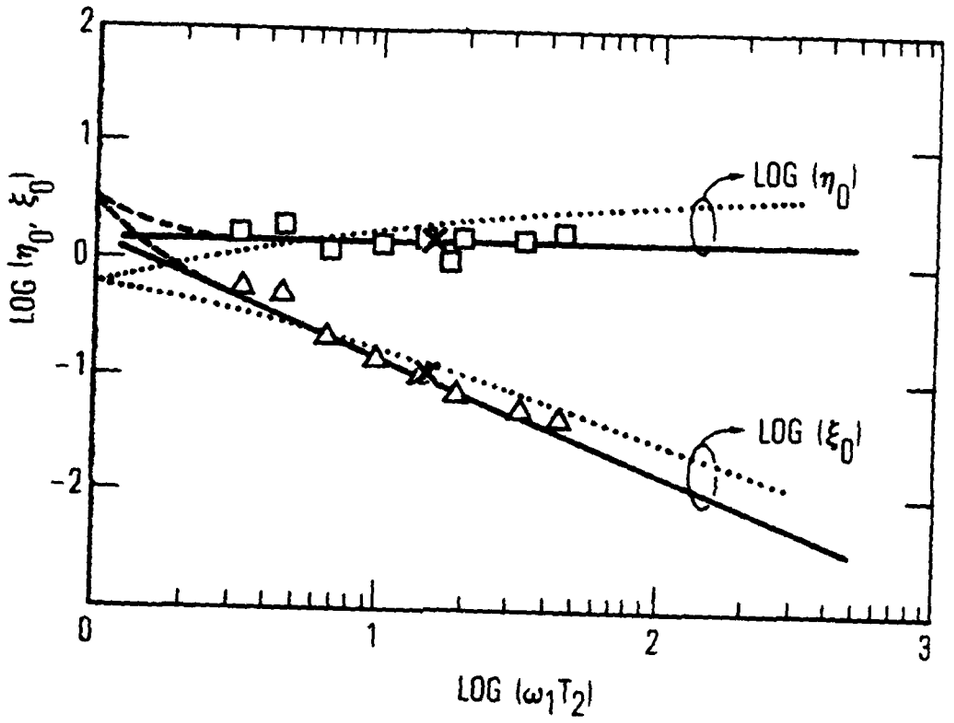

Fig. 5. Plots of the Adiabaticity Parameter η_0 and the Rapidity Parameter ξ_0 as Functions of the Normalized Rabi Frequency $\omega_1 T_2$. The boxes and triangles correspond to our measurements of the adiabaticity and rapidity parameters, respectively. The solid line represents the theoretical values obtained with the full ^{87}Rb density matrix, the dashed line corresponds to the spin-1/2 numerical solutions, and the dotted line corresponds to our approximate formula. The X's represent the data of Nakanishi et al., as explained in the text.

IV. THEORY

We have considered the ARP problem within three different theoretical frameworks: (1) a detailed density-matrix approach, where we include relaxation among the various sublevels and numerically solve the resulting coupled differential equations; (2) a two-level approximation of our system, where the coupled rate equations are solved numerically; and (3) an approximate analytical solution to the two-level problem. The first set of calculations allows us to make a comparison with experiment in order to determine the validity of both our experimental results and the theoretical model. By comparing the second set of calculations with the first, we can determine the degree to which our observations are generally valid. The last calculation, though approximate, is meant to provide physical insight into the theory, an insight not readily available from the numerical solutions.

A. THE ^{87}Rb DENSITY-MATRIX SOLUTION

The density-matrix equations used in the present calculation are essentially the same as those used previously by Camparo et al.,[11] except that we do not need to consider the effect of light shifts. The model assumes that all Zeeman sublevels of the $5^2S_{1/2}$ (F = 2) state have equal optical absorption rates, and that fluorescence repopulates the two ground-state hyperfine levels with equal probability at a rate much faster than does optical excitation. Furthermore, it is assumed that only two phenomenological relaxation rates are necessary to describe the ground state's return to its unperturbed state: a longitudinal relaxation rate γ_1 for the diagonal density-matrix elements, and a transverse relaxation rate γ_2 for the off-diagonal density-matrix elements. Lastly, since the microwaves are only in resonance with the 0-0 hyperfine transition, there are only two off-diagonal elements that need to be considered.

As discussed in Ref. 11, the symmetry of the model and the normalization of the density matrix reduces the complexity of the problem, so that we need only find solutions to five coupled differential equations:[15]

$$\dot{\rho} = - A\rho + R \tag{10}$$

with

$$\rho \equiv \begin{matrix} \rho(2,2) \\ \rho(2,0) \\ \rho(1,0) \\ \mathrm{Im}\ [\rho(2,0;1,0)] \\ \mathrm{Re}\ [\rho(2,0;1,0)] \end{matrix} \qquad R = \frac{\gamma_1}{8} \begin{matrix} 1 \\ 1 \\ 1 \\ 0 \\ 0 \end{matrix} \tag{11}$$

and

$$A \equiv \begin{matrix} \left(\frac{B}{2} + \gamma_1\right) & -\frac{B}{8} & 0 & 0 & 0 \\ -\frac{B}{2} & \left(\frac{7B}{8} + \gamma_1\right) & 0 & \omega_1 & 0 \\ -\frac{B}{2} & -\frac{B}{8} & \gamma_1 & -\omega_1 & 0 \\ 0 & -\frac{\omega_1}{2} & \frac{\omega_1}{2} & \left(\frac{B}{2} + \gamma_2\right) & \Delta(t) \\ 0 & 0 & 0 & -\Delta(t) & \left(\frac{B}{2} + \gamma_2\right) \end{matrix} \tag{12}$$

The instantaneous detuning between the hyperfine resonance and the microwave field is $\Delta(t)$, where

$$\Delta(t) = \Delta_0 - \beta t$$

and Δ_0 is the detuning at time $t = 0$; we assume a linear change in the microwave frequency with time: $d\omega/dt = \beta$.

These differential equations are solved numerically using Hamming's modified predictor-corrector method with a fourth-order Runge-Kutta starter.[16] We assume $\gamma_1 = \gamma_2$, and employ the values of B and γ obtained from the experiment. Δ_0 is chosen large enough so that the equation solutions at $t = 0$ can be well approximated by their off-resonance steady-state values. To determine the value of the sweep rate that maximizes the population reversal for a fixed Rabi frequency, the differential equations are solved, yielding the quantity

$$y(t_0) = 4\ \rho(2,2)_{t_0} + \rho(2,0)_{t_0} \tag{14}$$

for various values of β. $y(t)$ is the total density of the $F = 2$ hyperfine level, and t_0 is the time when this reaches a maximum. An example of the set of discrete data points generated in this way is shown in Fig. 6. A spline fit is then used to interpolate between these points in order to determine the theoretical value of β_0 for the particular Rabi frequency.[17] The theoretical values for the rapidity and adiabaticity parameters obtained in this way are plotted as a solid curve in Fig. 5.

B. THE TWO-LEVEL DENSITY MATRIX

The physics associated with this model is essentially the same as that described in the previous section, except that we now consider two states rather than eight. Letting the subscripts 1 and 2 denote the lower and upper hyperfine levels, respectively, we consider solutions to the three coupled rate equations:

$$\dot{\sigma}_{22} = \frac{\gamma_1}{2} - \left(\frac{B}{2} + \gamma_1\right)\sigma_{22} + \omega_1 \mathrm{Im}\,(\sigma_{21}) \tag{15a}$$

$$\mathrm{Re}(\dot{\sigma}_{21}) = -\left(\frac{B}{2} + \gamma_2\right) \mathrm{Re}(\sigma_{21}) + \Delta(t)\ \mathrm{Im}\,(\sigma_{21}) \tag{15b}$$

and

$$\mathrm{Im}\,(\dot{\sigma}_{21}) = -\left(\frac{B}{2} + \gamma_2\right) \mathrm{Im}(\sigma_{21}) - \Delta(t)\ \mathrm{Re}(\sigma_{21}) + \frac{\omega_1}{2}(1 - 2\sigma_{22}) \tag{15c}$$

where we have made use of the normalization condition: $\sigma_{22} + \sigma_{11} = 1$. The procedure for the numerical solution for β_0 is the same as before, except that we use a Runge-Kutta technique to solve the equations.[17] The calculated values of the rapidity and adiabaticity parameter for this model, which is essentially a Bloch model, are displayed in Fig. 5 as a dashed curve.

C. ANALYTIC APPROXIMATION

We now consider a spin-1/2 atom whose wavefunction is a linear combination of the spin-up and spin-down basis wavefunctions, χ_+ and χ_-:

$$\psi(t) = C_1(t)\chi_+ + C_2(t)\chi_- \tag{16}$$

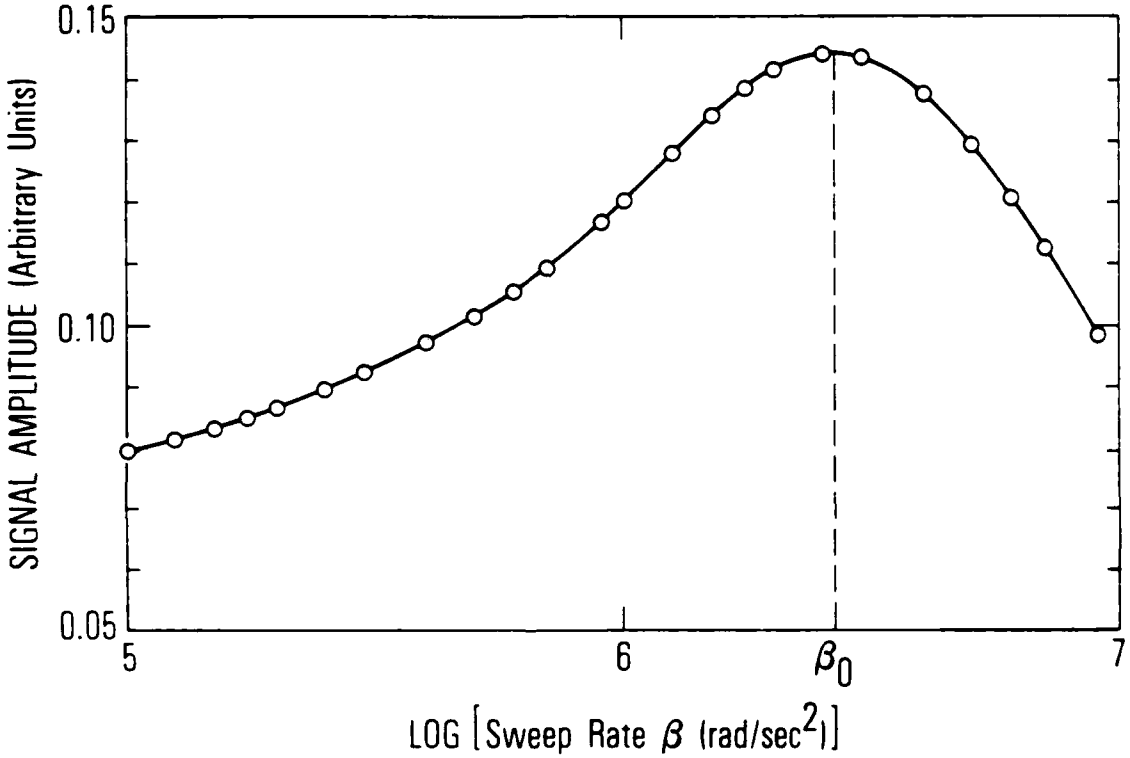

Fig. 6. An Example of the Discrete Set of Data Points Generated by our Model. The open circles correspond to the signal amplitude, in arbitrary units, calculated for a particular choice of the sweep rate β. The solid line is a spline fit of the numerical data points, allowing us to determine β_0.

We take the zero of energy for the atom as midway between the two states ($E_+ - E_- = h\omega_0$) and subject the atom to an oscillating electromagnetic field whose instantaneous frequency is changing at a rate β. If we ignore the counter-rotating component of the electromagnetic field, the wavefunction satisfies the Schrödinger equation

$$i\,h\,\dot{\psi}(t) = H(t)\psi(t) \tag{17}$$

where the Hamiltonian is

$$H(t) = \frac{h}{2}\begin{matrix} (\omega_0 - i\gamma) & \omega_1 \exp[-i(\omega_0 - \frac{\beta t}{2})t] \\ \omega_1 \exp[i(\omega_0 - \frac{\beta t}{2})t] & -\omega_0 \end{matrix} \tag{18}$$

and where we have included relaxation of the spin-up state in the form of an imaginary energy term, $-\frac{i\gamma h}{2}$. We will assume that for times very much before the passage through resonance the atom is in the spin-down state (i.e., $\lim_{t\to-\infty} |C_2(t)|^2 = 1$). After the passage through resonance there will be some nonzero probability of finding the atom in the spin-up state, but as $t \to +\infty$ this will decay to zero as a result of the damping term in the Hamiltonian.

Horwitz[18] has investigated a particular form of this problem, that of γ equal to zero. He found that in this case $|C_1(t)|^2$, a measure of the population reversal, may be expressed as a linear combination of two confluent hypergeometric functions. As t becomes large the reversal is complete and the asymptotic form of the solution may be used, yielding

$$\lim_{t\to\infty} |C_1(t)|^2 = [1 - \exp(-\pi\omega_1^2/2\beta)] \tag{19}$$

If γ is nonzero the problem is more complicated. However, when the sweep rate is more rapid than the relaxation rate, as it is for the cases we wish to consider, Horowitz states that Eq. (19) is only modified by the inclusion of an exponential decay term. Thus, in the presence of relaxation we expect

$$|C_1(t_m)|^2 \approx [1 - \exp(-\pi\omega_1^2/2\beta)]\,\exp(-\gamma t_m) \tag{20}$$

with t_m the time corresponding to maximum population reversal.

To specify t_m, use is made of our experimental observations. The maximum of the ARP signal occurs when the microwave frequency has swept beyond exact resonance by approximately the half width of the hyperfine line shape observed in slow passage (see Fig. 3). Thus, if we consider that the transition is power-broadened so that it has a FWHM of $2\omega_1$, then

$$t_m \simeq \omega_1/\beta \tag{21}$$

Furthermore, this value of t_m is consistent with the standard physical picture of ARP. Consider ARP in the rotating coordinate system in the absence of damping. As Fig. 7 shows, the atomic spin has a precessional frequency $\vec{\Omega}$:

$$\vec{\Omega} = \beta t\ \hat{z} + \omega_1\ \hat{x} \tag{22}$$

where the projection of $\vec{\Omega}$ onto the z axis determines the probability of finding the atom in a specific spin state. The important point to note, however, is that the projection of $\vec{\Omega}$ onto the z axis only changes appreciably near resonance. When the frequency has swept ω_1 beyond resonance, the population reversal is nearly 3/4 complete.

Substituting Eq. (21) into Eq. (20) results in an approximate expression for the maximum degree of population reversal. To determine the values of the rapidity and adiabaticity parameter, we need only find the solution to $\frac{d|C_1(t_m)|^2}{d\beta} = 0$ for a fixed Rabi frequency and relaxation rate:

$$\eta_0 = \frac{2}{\pi}\ \ell n\left(1 + \frac{\pi}{2}\frac{\omega_1}{\gamma}\right) \tag{23}$$

and

$$\xi_0 = \frac{2\gamma}{\pi\omega_1}\ \ell n\left(1 + \frac{\pi}{2}\frac{\omega_1}{\gamma}\right) \tag{24}$$

These values are also plotted in Fig. 5 as the dotted curve, where we have identified γ with the transverse relaxation rate.

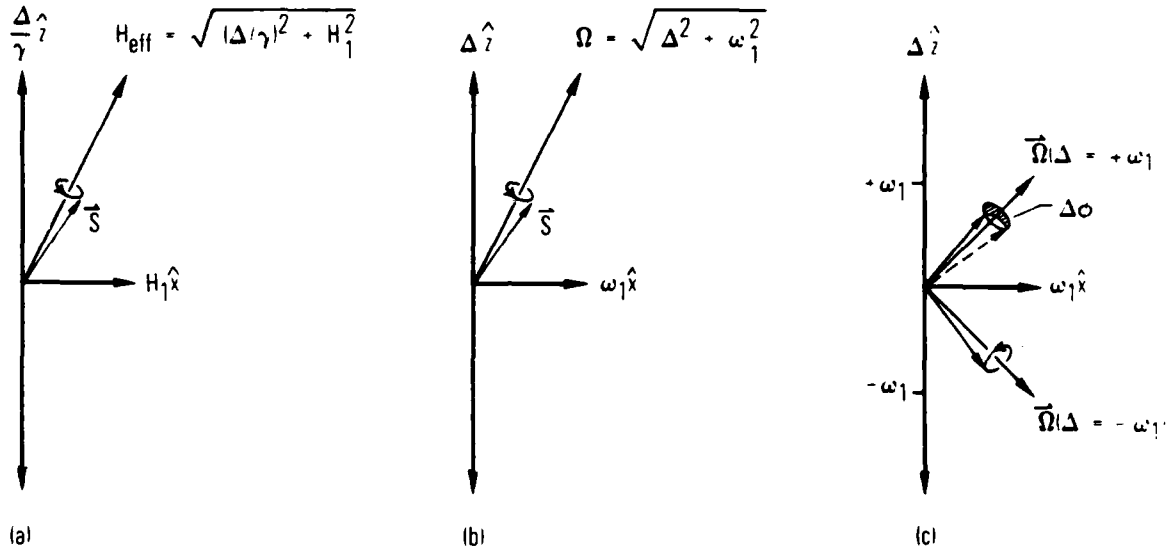

Fig. 7. In the Rotating Coordinate System the Spin Vector Precesses about an Effective Field H_{eff}, as Shown in (a); the Precessional Frequency is Ω, as Shown in (b); and (c) Depicts the Precessional Angle Swept Out during the Passage through Resonance, $\Delta\phi$, as the Effective Field is Swept from -z to +z.

V. DISCUSSION

A. COMPARISON OF THE EXPERIMENTAL RESULT AND THE FULL ^{87}Rb DENSITY-MATRIX CALCULATIONS

From Fig. 5 we see that the agreement between our experimental results and the ^{87}Rb theoretical model is quite good, and this indicates that at least on a formal level we have an accurate physical description of the rapidity and adiabaticity parameters. In particular, the theory supports our observation of the near constancy of the adiabaticity parameter, and yields the numerical relation

$$\omega_1^2/\beta \sim 1.5 \tag{25}$$

for this range of normalized Rabi frequency. This result then implies the inverse proportionality between the rapidity parameter and the normalized Rabi frequency:

$$\xi_0 = \frac{\eta_0}{\omega_1 T_2} \sim \frac{1.5}{\omega_1 T_2} \tag{26}$$

B. COMPARISON OF THE ^{87}Rb DENSITY-MATRIX CALCULATIONS AND THE SPIN-1/2 NUMERICAL SOLUTIONS

For $\omega_1 T_2 \gtrsim 3$ the numerical spin-1/2 calculations and the ^{87}Rb calculations show excellent agreement. In retrospect this should not have been too surprising; when the conditions for ARP are well satisfied, the extra Zeeman sublevels of the ^{87}Rb ground state are essentially decoupled from the two states interacting with the microwave field, and the ^{87}Rb atom behaves like a two-level system. Thus, it is more than coincidental that the agreement becomes good when ξ_0 becomes less than unity (i.e., when the passage through resonance becomes rapid). However, the disagreement for $\omega_1 T_2 < 3$ implies qualitatively different physics when the extra Zeeman levels of the ^{87}Rb ground state contribute to the ARP phenomenon. In this range of normalized Rabi frequency, intramultiplet relaxation becomes important.

The agreement between the two calculations also implies that the constancy of the adiabaticity parameter is a general phenomenon of ARP. To support this claim we note the recent experiment of Nakanishi et al.,[5] where the degree of population reversal in optical ARP was measured as a function of the resonance frequency sweep rate. The values of the rapidity and adiabaticity parameters obtained from their experimental results are represented by X's in Fig. 5. Furthermore, Ernst and Anderson[19] have performed numerical calculations to determine the sweep rate that maximizes the absorption mode signal in NMR, and have obtained a similar constant for the adiabaticity parameter. Finally, Antoniewicz and Ruijgrok[20] have suggested that in the absence of longitudinal relaxation, but in the presence of transverse relaxation, the adiabatic condition for population reversal is weaker than that defined by Eq. (2):

$$(\omega_1^2/\beta)^2 \gg 1 \tag{27}$$

C. QUALITATIVE ANALYSIS OF THE RESULTS

Our approximate formulas for the rapidity and adiabaticity parameters show reasonable agreement with the numerical calculations, considering the severity of the approximations used in deriving them, and should therefore contain qualitative information concerning the adiabaticity parameter's nearly constant value. Rewriting Eq. (20), we see that the maximum degree of population reversal is given by

$$|C_1(t_m)|^2 \sim [1 - \exp(-\pi\eta_0/2)]\ \exp(-\xi_0) \tag{28}$$

which can be thought of as the product of two probabilities. The first term is taken as the probability for an adiabatic passage,[21] and the second term as the probability for relaxation <u>not</u> to occur during the passage:

$$P_{\text{adiabatic}} \sim [1 - \exp(-\pi\eta_0/2)] \tag{29a}$$

and

$$P_{relax} \sim [1 - \exp(-\eta_0/\omega_1 T_2)] \tag{29b}$$

From the conditions for ARP as stated in Eq. (1), one would expect the degree of population reversal $|C_1(t_m)|^2$ to approach unity for some value of the sweep rate as the Rabi frequency becomes large, and from Eq. (28) this implies the following two limits:

$$\lim_{(\omega_1 T_2 \to \infty)} P_{adiabatic} = 1 \tag{30a}$$

and

$$\lim_{(\omega_1 T_2 \to \infty)} P_{relax} = 0 \tag{30b}$$

From Eq. (29a), the first of these limits implies that η_0 is an increasing function of the normalized Rabi frequency:

$$\lim_{(\omega_1 T_2 \to \infty)} \eta_0 = \infty \tag{31}$$

However, from Eq. (29b) and the second limit we have

$$\lim_{(\omega_1 T_2 \to \infty)} \frac{\eta_0}{\omega_1 T_2} = 0 \tag{32}$$

Now, using l'Hospital's rule,[22] we can obtain the limiting value for the rate at which the adiabaticity parameter changes as a function of normalized Rabi frequency:

$$\lim_{(\omega_1 T_2 \to \infty)} \frac{\eta_0}{(\omega_1 T_2)} = \lim_{(\omega_1 T_2 \to \infty)} \frac{[d\eta_0/d(\omega_1 T_2)]}{[d(\omega_1 T_2)/d(\omega_1 T_2)]} = \lim_{(\omega_1 T_2 \to \infty)} \frac{d\eta_0}{d(\omega_1 T_2)} = 0 \tag{33}$$

Thus, though the adiabaticity parameter is an increasing function of the normalized Rabi frequency, we would expect it to increase slowly; furthermore, it would appear that this is due to the necessity of minimizing the amount of relaxation that occurs during passage.

In order to understand the physical implication of the nearly constant value we have obtained for the adiabaticity parameter, we should review the physical content of the ARP adiabatic condition. Referring to Fig. 7, which shows the motion of a spin-1/2 system in the rotating coordinate system, the adiabatic condition states that the precessional frequency Ω should be large enough to allow the spin to follow changes in the direction of the effective field. Put differently, the precessional angle swept out by the spin in a time interval Δt should be of sufficient magnitude so that the spin can track the corresponding change in the direction of the effective field.[23]

We now denote by $\Delta\phi$ the angle through which the spin precesses in a time Δt ($\Delta\phi = \Omega\ \Delta t$) and consider a power-broadened transition of full width $2\ \omega_1$. The time it takes to cross the resonance is then $\Delta t = 2\ \omega_1/\beta$, and in that time the effective field has rotated by 90°. Near resonance we can assume that the precessional frequency is a minimum ($\Omega = \omega_1$) and that the precessional angle swept out by the spin is $\Delta\phi_r \sim 2(\omega_1^2/\beta)$. If $\Delta\phi_r$ is to be large enough so that the spin tracks the 90° change in the direction of the effective field, then the adiabaticity parameter must be larger than some minimum value.

From the fact that the adiabaticity parameter is constant over such a wide range of Rabi frequency, where we know the spin is following the effective field (i.e., we can see the effects of the population reversal), we must assume that the minimum value of the adiabaticity parameter is ~1.5. This would then imply that the minimum precessional angle necessary for the spin to track a 90° change in the direction of the effective field is three radians, or approximately a half revolution. This is a very surprising result, since we would have imagined that many revolutions would be required to track a 90° change in the direction of the effective field; yet the above argument indicates otherwise.

VI. SUMMARY

In conclusion, we have investigated ARP in the 0-0 hyperfine transition of ^{87}Rb. In particular, we have measured and calculated the value of the adiabaticity parameter that maximizes the degree of population reversal as a function of normalized Rabi frequency. We find that this value is nearly constant over the range of normalized Rabi frequencies considered, with a value of ~1.5. The reason for its constancy seems to be due to the necessity of minimizing the amount of relaxation that occurs during the passage. Furthermore, the result implies that for a two-level system a precession of only half a revolution about the effective field is sufficient for the spin vector to follow a 90° change in the direction of the effective field. Through our calculations and comparisons of the present results with other ARP experiments, we have demonstrated the applicability of our conclusions to ARP in general.

REFERENCES

1. F. Bloch, Phys. Rev. 70, 460 (1946).

2. A. Abragam, The Principles of Nuclear Magnetism (Oxford University Press, Oxford, 1961), pp. 34-36.

3. G. E. Pake, Paramagnetic Resonance (W. A. Benjamin, Inc., New York, 1962) pp. 21-30.

4. M. M. T. Loy, Phys. Rev. Lett. 32, 814 (1974).

5. S. S. Nakanishi, T. Endo, T. Muramoto, and T. Hashi, Optics Comm. 31, 419 (1981).

6. M. M. T. Loy, Phys. Rev. Lett. 41, 473 (1978).

7. R. Bernheim, Optical Pumping (W. A. Benjamin, Inc., New York, 1962).

8. L. C. Balling, in Advances in Quantum Electronics, ed. D. W. Goodwin, (Academic Press, New York, 1975), Vol. 3, pp. 1-167.

9. W. Happer, Rev. Mod. Phys. 44, 169 (1972).

10. This value was determined by using Beer's Law at low light intensity so that there was no observable optical pumping: $\ln [I(\text{off resonance})/I(\text{on resonance})] = \frac{3}{8} [Rb]\sigma\ell$.

11. J. C. Camparo, R. P. Frueholz, and C. H. Volk, Phys. Rev. A 27, 1914 (1983).

12. J. D. Jackson, Classical Electrodynamics (John Wiley & Sons, Inc., New York, 1975), pp. 353-356.

13. J. C. Camparo and R. P. Frueholz (manuscript in preparation).

14. This value implies that $\langle \vec{I} \cdot \vec{S} \rangle$, the measure of hyperfine polarization, was -0.63.

15. We define the density-matrix nomenclature as follows: $\rho(F, m_F) = \delta_{FF'}\delta_{m_F m_F'}$ $\rho(F, m_F; F', m_F') = \delta_{FF'}\delta_{m_F m_F'} \langle F, m_F|\rho|F', m'_F\rangle$

16. B. Carnahan, H. A. Luther, and J. O. Wilkes, Applied Numerical Methods (John Wiley & Sons, Inc., New York, 1969), pp. 341-428.

17. R. H. Pennington, Introductory Computer Methods and Numerical Analysis (The MacMillan Co., Collier-MacMillan Canada, Ltd., Toronto, 1970).

REFERENCES (Continued)

18. P. Horwitz, Appl. Phys. Lett. 26(6), 306 (1975); see also A. M. F. Lau, Phys. Rev. A 14, 279 (1976).

19. R. R. Ernst and W. A. Anderson, Rev. Sci. Instr. 36 (12), 1996 (1965).

20. P. R. Antoniewicz and Th. W. Ruijgrok, Physica 52 (1), 153 (1971).

21. C. Zener, Proc. Roy. Soc. 137, 696 (1932).

22. L. Bers, Calculus (Holt, Rinehart and Winston, Inc., New York, 1969), p. 549.

23. J. G. Powles, Proc. Phys. Soc. (London) 71, 497 (1958).

24. F. A. Franz, Phys. Rev. A 6, 1921 (1972).

APPENDIX: THE RELATION OF THE TRANSMISSION LINE SHAPE LINEWIDTH TO THE PEAK AXIAL MICROWAVE RABI FREQUENCY

In the present experiment we used the transmission line shape linewidth to measure the microwave Rabi frequency. However, since the experiment employed a TE_{011} cavity with its concomitant mode structure, and because it is not valid to assume that the motion of the atoms performs a complete averaging of the microwave field,[11] care must be exercised in interpreting the measurement of the Rabi frequency by this method. As stated in the text, the radial distribution of the microwave power can be considered as essentially uniform. However, the longitudinal dependence of the microwave field has the form $\sin(\frac{\pi z}{L})$, where L is the length of the cavity and z is the axial position in the cavity measured from the front face. In this appendix we present an argument to show that in our experiments the transmission line shape linewidth provides a reasonable measurement of the peak axial microwave Rabi frequency.

For simplicity, consider the transmission line shape for an optically pumped spin-1/2 atom. It is quite easy to show that the transmitted light intensity as a function of microwave detuning Δ is given by an expression of the form

$$I(\Delta) = I_0 \exp\left[-N\sigma \int_0^L \zeta(\Delta,z)\, dz\right] \tag{A1}$$

where N and σ are the number density and absorption cross section, respectively. $\zeta(\Delta,z)$ is the fraction of atoms in the absorbing state as a function of axial position and detuning:[8]

$$\zeta(\Delta,z) = \frac{1}{2}\left(\frac{\gamma}{R+\gamma}\right)\left[1 + \frac{R}{\gamma}\frac{\omega_1^{\,2}}{(R+\gamma)^2 + \Delta^2 + \omega_1^{\,2}}\right] \tag{A2}$$

where R and γ are the pumping and relaxation rates, respectively. The signal is the change in the transmitted intensity as the microwaves are swept across resonance: $S = [I(\Delta = \infty) - I(\Delta)]$.

If the vapor is optically thin, then the signal takes on a fairly simple form:

$$S \sim \int_0^L \left(\frac{R}{R+\gamma}\right) \left[\frac{\omega_1^2}{(R+\gamma)^2 + \Delta^2 + \omega_1^2}\right] dz \tag{A3}$$

Furthermore, by having an optically thin vapor we can assume that the pumping rate is constant over the length of the cell, which thus leaves the Rabi frequency as the only variable dependent on the axial position. Replacing ω_1 by $\omega_{1p} \sin(\pi z/L)$ (i.e., the atoms are rigidly frozen in place because of the presence of a buffer gas), we have

$$S \sim \int_0^L \left[\frac{\omega_{1p}^2 \sin^2(\pi z/L)}{(R+\gamma)^2 + \Delta^2 + \omega_{1p}^2 \sin^2(\pi z/L)}\right] dz \tag{A4}$$

Evaluating the integral yields

$$S \sim \pi\,(1 - \sqrt{x}) \tag{A5}$$

with

$$x \equiv \frac{(R+\gamma)^2 + \Delta^2}{(R+\gamma)^2 + \Delta^2 + \omega_{1p}^2} \tag{A6}$$

Though the signal line shape expressed by Eq. (A5) does not have a particularly appealing form, it is quite easy to show that when conditions are chosen so that x approaches unity, the signal line shape is Lorentzian:

$$S \simeq \frac{\pi}{2} \left[\frac{\omega_{1p}^2}{(R+\gamma)^2 + \Delta^2 + \omega_{1p}^2}\right] \tag{A7}$$

From Eq. (A6) it is clear that Eq. (A7) is a good approximation of the predicted signal when $[\omega_{1p}/(R+\gamma)]^2 \ll 1$ and/or is in the wings where $(\omega_{1p}/\Delta)^2 \ll 1$. Furthermore, it is obvious that the linewidth of the approximating Lorentzian is

$$\Delta_{1/2}^2 = (\mathrm{HWHM})^2 = (R + \gamma)^2 + \omega_{1p}^{\ 2} \tag{A8}$$

In Fig. A-1 we show the line shape predicted from Eq. (A5) under the high microwave power conditions of the present experiment, along with the approximating Lorentzian of Eq. (A7). Though the linewidths of the two line shapes differ by roughly a factor of two, it should be noted that there is good agreement in the wings where Eq. (A7) is valid. Therefore, if the above discussion of the signal line shape contains a complete description of the relevant physics, then we must conclude that the linewidth of the transmission signal does not represent a good measure of ω_{1p}; rather, one should obtain this quantity by examining the line shape wings. However, if we consider more closely the physical assumptions made in writing Eq. (A2), we realize that the analysis of the line shape presented in this appendix does not consider the boundary conditions on ζ imposed by the walls of the absorption cell.[24] It might be reasonable to ignore these boundary conditions when $R \gg \gamma$ (i.e., when the distribution of hyperfine polarization is nearly constant over the entire length of the cell, abruptly falling to zero at the walls), but one cannot expect this to be a reasonable assumption under the conditions of the present experiment, where $R \gtrsim \gamma$. In fact, under the conditions of the present experiment one would expect the spatial regions furthest from the walls to contain the greatest degree of hyperfine polarization, so that these regions should be weighted more heavily in the integral of Eq. (A4).

Figure A-2 shows the experimental slow-passage line shape under conditions of high microwave power along with a Lorentzian fit of the data in the wings. (The data are a signal average of 1000 slow passages through resonance.) As can be seen, the agreement between the experimental line shape and the approximating Lorentzian is much better than Eq. (A5) would lead one to expect. As mentioned above, the reason for the better agreement lies in the fact that at low light intensity most of the signal comes from the spatial

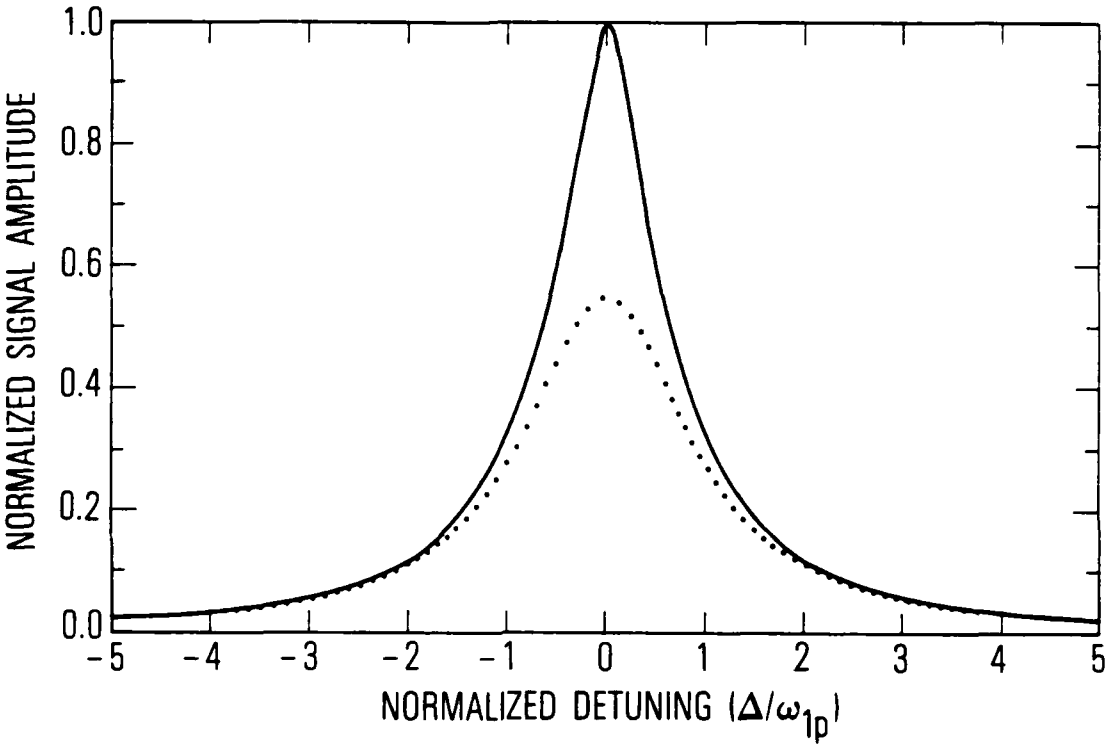

Fig. A-1. The Predicted Line Shape (solid curve) when the Axial Variation of the Microwave Rabi Frequency is Considered, as Discussed in the Appendix, and a Lorentzian (dotted curve) that Approximates This Line shape in the Wings.

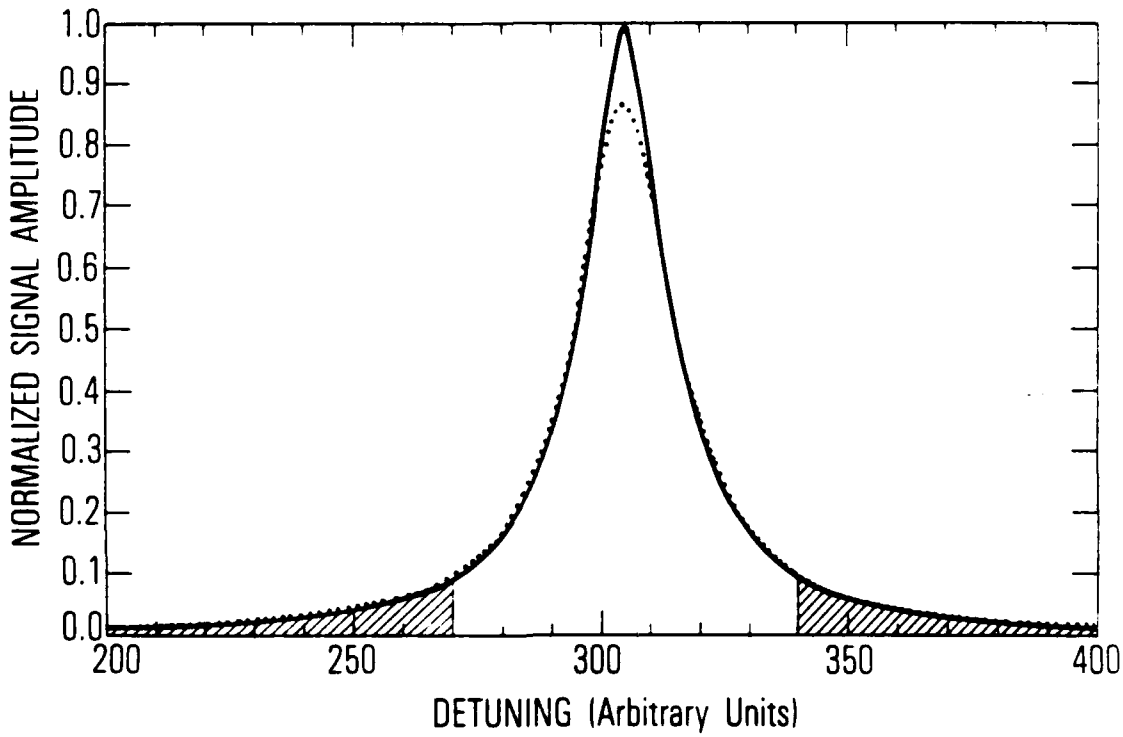

Fig. A-2. The Slow-Passage Experimental Line Shape (solid curve) for High Microwave Power, and a Least-Squares Lorentzian Fit (dotted curve) to the Wings (hatched areas). The reasonable agreement between the two curves indicates that the HWHM of the experimental line shape is a fairly accurate measure of ω_{1p}.

regions furthest from the walls. It is a coincidence of the TE_{011} mode structure that the regions expected to contain the smallest values of ζ correspond to the regions where $\omega_1(r,z) \approx \omega_{1p}$. Thus, we make the approximation that the HWHM of the experimental line shape is indicative of ω_{1p}, and Fig. A-2 indicates that this will lead to $\lesssim$ 10% error, which is insignificant on the log plot of Fig. 5.

LABORATORY OPERATIONS

The Laboratory Operations of The Aerospace Corporation is conducting experimental and theoretical investigations necessary for the evaluation and application of scientific advances to new military space systems. Versatility and flexibility have been developed to a high degree by the laboratory personnel in dealing with the many problems encountered in the nation's rapidly developing space systems. Expertise in the latest scientific developments is vital to the accomplishment of tasks related to these problems. The laboratories that contribute to this research are:

Aerophysics Laboratory: Launch vehicle and reentry fluid mechanics, heat transfer and flight dynamics; chemical and electric propulsion, propellant chemistry, environmental hazards, trace detection; spacecraft structural mechanics, contamination, thermal and structural control; high temperature thermomechanics, gas kinetics and radiation; cw and pulsed laser development including chemical kinetics, spectroscopy, optical resonators, beam control, atmospheric propagation, laser effects and countermeasures.

Chemistry and Physics Laboratory: Atmospheric chemical reactions, atmospheric optics, light scattering, state-specific chemical reactions and radiation transport in rocket plumes, applied laser spectroscopy, laser chemistry, laser optoelectronics, solar cell physics, battery electrochemistry, space vacuum and radiation effects on materials, lubrication and surface phenomena, thermionic emission, photosensitive materials and detectors, atomic frequency standards, and environmental chemistry.

Computer Science Laboratory: Program verification, program translation, performance-sensitive system design, distributed architectures for spaceborne computers, fault-tolerant computer systems, artificial intelligence and microelectronics applications.

Electronics Research Laboratory: Microelectronics, GaAs low noise and power devices, semiconductor lasers, electromagnetic and optical propagation phenomena, quantum electronics, laser communications, lidar, and electro-optics; communication sciences, applied electronics, semiconductor crystal and device physics, radiometric imaging; millimeter wave, microwave technology, and RF systems research.

Materials Sciences Laboratory: Development of new materials: metal matrix composites, polymers, and new forms of carbon; nondestructive evaluation, component failure analysis and reliability; fracture mechanics and stress corrosion; analysis and evaluation of materials at cryogenic and elevated temperatures as well as in space and enemy-induced environments.

Space Sciences Laboratory: Magnetospheric, auroral and cosmic ray physics, wave-particle interactions, magnetospheric plasma waves; atmospheric and ionospheric physics, density and composition of the upper atmosphere, remote sensing using atmospheric radiation; solar physics, infrared astronomy, infrared signature analysis; effects of solar activity, magnetic storms and nuclear explosions on the earth's atmosphere, ionosphere and magnetosphere; effects of electromagnetic and particulate radiations on space systems; space instrumentation.

END

FILMED

10-85

DTIC